The effect of the martensitic packet size on the machinability of modified AISI P20 prehardened mold steel

H. Hoseiny[a]*, F. G. Caballero[b], B. Högman[a], D. San Martin[b], C. Capdevila[b], L.-G. Nordh[a], H.-O. Andrén[c]

[a] *Research and Development, Uddeholms AB, SE-683 85 Hagfors, Sweden*

[b] *Department of Physical Metallurgy, Centro Nacional de Investigaciones Metalúrgicas (CENIM-CSIC), Avda. Gregorio del Amo 8. E-28040 Madrid, Spain*

[c] *Department of Applied Physics, Chalmers University of Technology, SE-412 96 Göteborg, Sweden*

*Corresponding author:

Hamed Hoseiny

Research & Development

Uddeholms AB

SE-683 85 Hagfors

Sweden

Phone: +46 (563) 17885

Mobile: +46 707 139733

Emails: hamed.hoseiny@uddeholm.se; smhh@alumni.chalmers.se

Abstract The effect of martensitic packet size on the machinability of a prehardened mold steel at a hardness of ~ 40 HRC (typical hardness for prehardened mold steels) was studied in terms of cutting force and tool life. The machinability tests were performed in end milling using coated cemented carbide tools at three different cutting speeds. The results showed that an increase in the martensite packet size led to higher cutting force and shorter tool life. The increase in cutting force was related to the increase of work hardening. The work material with a coarser martensite packet size showed a higher amount of work hardening that can explain the higher cutting force. The longer tool life in the workpieces with finer structure was correlated to smaller amplitude of the variation in cutting force.

Keywords: *Machinability, end milling, prehardened mold steel, martensite packet size, prior austenite grain size*

1. Introduction

The demand for prehardened mold steels has greatly increased due to their more practical and economic efficiency over the post roughing hardened steels. The former are machined after they are hardened to the final in-service hardness while the latter are machined (rough machining) in the soft annealed condition prior to hardening. Hence, among the many properties required from these steels, machinability is of crucial importance since machining is the most costly process in manufacturing of molds [1-4].

It is well known that microstructure has a great influence on the machinability of steels [5-7] and grain size is one the microstructural features that has a major influence on properties of workpiece material. Hence, investigation on the effect of the grain size on machinability has attracted considerable interest [8-14]. However, there are few systematic investigations since grain coarsening may reduce the hardness that directly affects the machinability and obstructs the independent study of the role of grain size. Early studies by Thoors [13] on the effect of prior austenite grain size in turning of a microalloyed forging steel with high speed steel (HSS) tools showed a better machinability with coarser grains at high material removal rate (MRR) i.e. higher feed rate and depth of cut, while better machinability was seen with smaller grains at lower MRR. Vojcak [14] studied the machinability of AISI 1018 carbon steel under various microstructural conditions in plunge turning by HSS tools. It was observed that increasing the grain size from 20 μm to 56 μm reduced the tool wear by 10-50 % depending on structure.

Most of these studies have been focused on ferritic-pearlitic or austenitic steels, but steels with a martensitic microstructure have not been considered in this respect. Moreover, the machinability has been tested mainly in turning as a continuous cutting process but interrupted cutting operations such as milling have not been sufficiently studied.

One of the main characteristics that may cause martensitic microstructures to behave differently from others is its specific substructure within the prior austenite grains. Lath martensite is the

typical microstructure for modified AISI P20 alloy in hardened (quenched and tempered) condition [15,16]. In this kind of steels a prior austenite grain is divided into several packets which are group of laths with the same habit plane [17,18] and packets are subdivided into blocks, which consist of laths with a small misorientation [19-23].

It is widely accepted that martensitic packet and block boundaries have high angle misorientation and therefore the packets and blocks are considered as effective grain sizes in lath martensitic structures that contribute to mechanical properties e.g. strength [24-27]. Therefore, apart from the prior austenite grain size, packet and/or block size should be considered as relevant parameters to correlate microstructure with machinability in lath martensitic structures.

In the present work, the machinability of modified AISI P20 mold steel at prehardened condition (~ 40HRC) with different prior austenite grain and packet sizes is examined in end milling as one of the most feasible machining operations in mold making. The machinability is studied in terms of cutting force and tool life and the results are related to the microstructural characteristics.

2. Experimental Procedure

2.1 Material and heat treatments

The chemical composition of the steel is given in Table 1. The steel is Uddeholm Impax HH that resembles modified AISI P20. It was hot rolled to a cross section of 50 mm × 200 mm, followed by a stress relieving treatment at 650˚C for 9 hours and air cooling to room temperature. For machinability and mechanical tests, workpieces of 50 mm × 100mm × 200 mm were austenitized at 900˚C, 950˚C, 1000˚C and 1050˚C (designated $T_\gamma 900$, $T_\gamma 950$, $T_\gamma 1000$ and $T_\gamma 1050$, respectively) for 30 min in order to obtain different prior austenite grain sizes followed by quenching in oil and double tempering at 540˚C for 2 × 2 hours. A hardness of 40-42 HRC was reached for all treated workpieces.

2.2. Microstructural characterization

Prior austenite grain boundaries were revealed by the thermal etching method [28,29]. For this purpose, a 2 mm wide and finely polished surface was created along the longitudinal axis of

cylindrical samples 4 mm in diameter and 10 mm in length. Samples were austenitized in a radiation furnace at the selected temperatures and subsequently cooled down to room temperature at a rate of 10˚C/s. This method involves preferential transfer of material away from the grain boundaries when the steel is exposed to a high temperature in an inert atmosphere. Thus, during austenitization of a pre-polished sample, grooves are formed at the intersections of the prior austenite grain boundaries with the polished surface. As optical micrographs in Fig. 1 illustrate, these grooves remain intact and are clearly visible after cooling to room temperature, outlining the prior austenite grain boundaries. The prior austenite grain size was measured on these optical micrographs using the Nomarski differential interference contrast microscopy technique [30] on a light optical microscope (LOM). The equivalent circular diameter of about 230 prior austenite grains was measured for each treated sample and the mean grain size was calculated.

Determination of martensitic packets was done by Electron Channeling Contrast (ECC) [31,32] on quenched and tempered samples. Samples were polished to 1 μm diamond paste, followed by polishing with colloidal silica to remove any possible mechanical damage from former metallographic preparation steps. The packets were revealed using a JEOL JSM-6500F field emission gun scanning electron microscope (FEG-SEM) in backscatter mode. The packet size was measured by linear intercept method on the micrographs. Figure 2 shows the packet boundaries in the micrographs of quenched and tempered samples.

A 2 % Nital etching solution was also used to reveal the microstructure of quenched and tempered material in an FEI Quanta 600 F FEG-SEM in secondary electron mode.

Quantitative X-ray diffraction analyses were made to determine the fraction of retained austenite. For this purpose, 15 mm × 35 mm × 10 mm (width × length × thickness) samples were machined. After grinding and final polishing using 1 μm diamond paste, the samples were electropolished to obtain an undeformed surface. They were then step-scanned in a XRD 3003 PTS diffractometer using unfiltered Cr Kα radiation. The scanning speed (2θ) was less than 0.3 degree/min. The machine was operated at 40 kV and 30 mA. The volume fraction of retained austenite was calculated from the integrated intensities of (111), (200) and (220) austenite peaks, and those of (110), (200) and (211) peaks of ferrite.

2.3. Machinability tests

The machinability tests were conducted on a three axis CNC, Modig 7000 Machining Center, with maximum power of 10 kW and spindle speed of 15000 rpm. The cutting tool was a Sandvik Coromant R390-016A16-11L with a diameter (D_c) of 16 mm, tool cutting edge angle (κ_r) of 90˚ and inclination angle (λ_s) of 13.43˚. The inserts were of Coromant R390-11 T3 08M-PL 1030 WC-Co type cemented carbide type with PVD TiAlN multilayer coating. The cutting parameters for the machining experiments are given in Table 2.

The cutting forces were measured with the help of a piezoelectric three-component Kistler dynamometer type 9257A at a sampling rate of 25.6 kHz. The measurements were done on 38 mm long pieces cut from the heat treated specimens using a new insert to eliminate any influence from wear on the cutting forces.

Tool life tests have been performed on the heat treated blocks with the criterion of 0.2 mm maximum flank wear (VB = 0.2 mm).

2.4. Mechanical testing

Tensile properties and Charpy-V impact toughness were measured as they can influence the machinability [33,34]. Tensile tests were performed according to EN 10002–1:2001 standard on a Zwick Z250/SW5A machine with a maximum load of 250 kN. Samples were cut in two orientations of LT (long-transverse) and TL (transversal-long). Three tests were performed for each heat treatment and orientation at room temperature.

Charpy-V notch impact tests were performed in a Roell Amsler RK150 machine with nominal energy of 150 J and release angle of 150˚, according to standard EN 10045. Similar to tensile tests, the Charpy-V impact tests were carried out for two specimen orientations and repeated three times for every heat treatment.

3. Results and Discussion

3.1. Microstructure and mechanical properties

Figure 3(a) shows the variation of prior austenite grain and packet size with austenitization temperature. As expected, the size of prior austenite grains increases as austenitization temperature increases. Their corresponding error bars are standard deviations of the mean value. It should be noticed that the larger number of annealing twin boundaries in the microstructure of Tγ1050 sample (see Fig. 1(d)) is associated with coarser prior austenite grains as is well established in the literature [35,36].

Figure 3(b) shows a nearly linear relationship between the size of the prior austenite grains and that of packets. The equation related to the solid line is represented next to it in the same figure. It is also well established that the packet size increases linearly with prior austenite grain size [25,26,24].

Figure 4 shows the martensitic microstructure after quenching and tempering. It consists of tempered martensite and a fine distribution of carbide particles precipitated within the martensite laths and carbide films formed at the lath boundaries. The nature of these carbides was found to be M_3C as reported elsewhere [15]. As can be seen in the micrographs there is no significant difference in steel microstructure in terms of carbide distribution and size, since all samples were tempered at the same conditions and the majority of the primary carbides are dissolved during austenitization. The amount of retained austenite in all heat treated steel samples was determined by XRD to be less than 1% after tempering.

Tensile test results listed in Table 3 suggest that there is no significant effect of the austenitization temperature on the yield strength and the tensile strength. On the other hand, ductility (elongation and reduction of area) and impact toughness had improved for lower austenitization temperatures. It is well established that the packet size controls the toughness of steels with an inverse effect [26,37]. The reduction of the tensile ductility with an increase of the packet size has also been reported previously [38].

3.2. Machinability: Cutting force

For the evaluation of cutting force, the resultant cutting force (F_{xy}) is calculated using the Pythagorean equation:

$$F_{xy} = \sqrt{F_x^2 + F_y^2} \qquad (1)$$

where F_y and F_x are cutting force components in the feed direction and normal to the feed direction in the plane of cutting, respectively, which are the main cutting force components in milling operations [33,39].

3.2.1. Effect of packet size

Fig. 5(a) shows the effect of the packet size on the cutting force at different cutting speeds. It can be seen that generally the cutting force rises with an increase in packet size; yet, this effect is dependent on the cutting speed. At the lower cutting speed (120 m/min) the cutting force is less sensitive to the packet size. A slightly higher force (still within the standard deviation) during cutting of $T_\gamma 950$ compared to $T_\gamma 1000$ is probably due to the larger yield strength of $T_\gamma 950$. It is well known that the shear force required to form a chip increases as the yield strength of work material rises [40]. Hence, the effect of a smaller packet size in $T_\gamma 950$ on the cutting force reduction is compensated by its larger yield strength. Nevertheless, at the two higher cutting speeds, the cutting force increases linearly with packet size, except for $T_\gamma 1050$ (the largest packet size) at the highest cutting speed (200 m/min). It can be seen that the cutting force drops abruptly at this point. In order to examine the reproducibility of this result, the test was repeated under the same conditions and similar results were obtained, confirming that this drop in cutting force is not due to an experimental error. It is noteworthy to mention that there was, to some extent, a better correlation between the cutting force and packet size than with the prior austenite grain size.

The increment of the cutting force with packet size can be attributed to the increase in the degree of work hardening. The cutting force is larger the smaller the shear plane angle is [41,40] and the shear plane angle reduces as the work hardening becomes larger in the primary shear zone in the chip [41,42]. Accordingly, Childs et al. [41] have considered the $(k_{max} - k_o)/k_{max}$ (where k_0 and k_{max} are the shear stresses at the entry and exit to the primary shear plane , respectively) as an indicator for machinability of materials as far as tool forces and stresses and power consumption are concerned. Fig. 6 shows a linear relation between the work hardening ratio, determined by $R_m/R_{p0.2}$, and the reciprocal square root of the packet size. It indicates that the work hardening

ratio increases as the packet size becomes coarser. The work hardening decrease accompanying a reduction of the grain size in fine-grained steels (20 nm – 20 μm) has been confirmed by Tomota et al. [43]; however, there is not much information available on this effect in martensitic steels.

3.2.2. Effect of cutting speed

In Fig. 5(b) the effect of the cutting speed on the cutting force is illustrated for each heat treated condition. It shows that the steel response to variation of the cutting speed differs with the size of prior austenite grain and/or packet. It is a common experience that the cutting force decreases when the cutting speed increases, mainly due to temperature rise and thermal softening of the work material and, consequently, of the shear angle expansion [42]. However, the strain and strain rate increase at higher cutting speeds, results in larger flow stress and work hardening. Consequently, depending on the material and the cutting parameters, the interplay between the work hardening and thermal softening may lead to higher hardness, causing an increase of the cutting force when raising the cutting speed in a specific range, as it is observed likewise by other researchers [44]. In this manner, an increase of cutting force during the machining of $T_{\gamma}1000$ and $T_{\gamma}1050$ with cutting speed in a particular range could be explained in this way considering their higher work hardening ratio. The abrupt reduction of the cutting force for $T_{\gamma}1050$ below that found for $T_{\gamma}1000$ for the cutting speed of 200 m/min can probably be correlated to temperature rise and domination of thermal softening. The higher cutting temperature for milling of $T_{\gamma}1050$ compared to the other heat treated conditions at the cutting speed of 200 m/min could be recognized clearly from the color of the chips. Evidently the higher work hardening of the workpiece generates a higher cutting temperature.

3.3. Machinability: Tool life

The tool life test results for different cutting speeds are demonstrated in Fig. 7. Considering the regular scatter in the tool life machining test, the difference between the different heat treated workpieces in terms of tool life at cutting speed of 200 m/min is marginal. Nevertheless, for the two lower cutting speeds it is obvious from the overall results that a longer tool life is obtained when milling finer-grained workpieces ($T_{\gamma}900$ and $T_{\gamma}950$). At the cutting speed of 120 m/min, the

notch wear was the failure mechanism for the sample $T_\gamma 900$ (see Fig. 8), however, the flank wear which was the tool performance criterion in this work, lies below the one for $T_\gamma 950$ all the way before notch happens. It can be concluded that $T_\gamma 900$ sample is still superior to the sample $T_\gamma 950$ by the criterion used for tool life tests in the current study. It is known that larger cutting forces lead to more wear by imposing higher stresses and high tensile stresses can break up the WC grains of the carbide tool into fragments which are carried away by the flowing metal. Accordingly, the lower cutting forces can be counted as one of the reasons for longer tool life in finer-grained heat treated workpieces; although there are more factors, such as cutting temperature, which deteriorate the tool performance. As the cutting speed increases, the cutting temperature raises resulting in softening and consequently early failure of the cutting tool. As a result, at higher cutting speed, the tool performance is more controlled by the tool material than the work material. This can be a reason for the decline in difference between heat treatments in terms of tool life with increasing the cutting speed.

Nevertheless, as mentioned before, the difference in cutting forces especially between the samples $T_\gamma 900$, $T_\gamma 950$ and $T_\gamma 1000$ is minimal while the tool life of $T_\gamma 1000$ and $T_\gamma 1050$ samples are considerably lower than the other finer-grained specimens. Hence, the difference in the cutting force merely cannot explain the observed differences in the tool lives. Jiang et al. [9] have studied the effect of grain size on the machinability of austenitic stainless steels in terms of chip formation and tool life. Their results have shown shorter tool life as grain size increases which is attributed to the higher work hardening of the workpiece associated with coarser grain size and consequently more abrasive wear. Moreover, the higher cutting temperature due to the higher work hardening led to more diffusion wear. It is also shown that a larger grain size distribution reduces the tool life by increasing the cutting force amplitude. The chip segment height ratio (ratio between the minimum and maximum height of the chip) increases with grain size [8,9]. In addition, the scatter in chip segment height ratio increases as the grain size distribution enlarges, leading to a more inhomogeneous deformation of work material [45,8] and as a result a larger amplitude of cutting force variation, which accelerates the tool wear. Accordingly, the higher cutting force amplitude can be counted as another reason for shorter tool life when machining the workpieces with larger packet size. The increase in amplitude of cutting force with austenitization temperature is shown in Fig. 7(d). As it is indicated by the error bars in Fig. 3(a), the distribution of prior austenite grains becomes larger as the austenitization temperature

increases, and the corresponding packet size distribution is expected to be wider after austenitizing at higher temperatures. This can explain the increase of cutting force amplitude with austenitization temperature.

4. Conclusions

The effect of the austenitization temperature on machinability is examined in terms of cutting force and tool life in end milling of a modified AISI P20 in prehardened condition. The main conclusions are:

- The cutting force generally increases with the martensitic packet size, with the exception of the largest packet size at the highest cutting speed.
- The increase of the cutting force with the packet size is associated with an increase in the degree of work hardening in the work material.
- The tool life was longer for the workpieces with smaller packet size, which is correlated to the lower cutting force and smaller amplitude in variation of cutting force.

Acknowledgements The authors gratefully acknowledge the financial support of Uddeholms AB, Vinnova within Vinnpro program and CAPE research center. Rickard Sundström (Sandvik Tooling) is thanked for providing the cutting tools and helpful recommendations regarding machining tests. H. Hoseiny thanks Centro Nacional de Investigaciones Metalúrgicas (CENIM-CSIC) for providing the opportunity to carry out part of this investigation using their experimental facilities.

References

1. Hippenstiel F (ed) (2004) Handbook of Plastic Mould Steels. Edelstahlwerke Buderus AG, Wetzlar
2. Hoseiny H (2009) Metallurgical Aspects of Machinability of Prehardened Mould Steels. Licentiate of Engineering Thesis. Chalmers University of Technology, Göteborg
3. Zinner S, Perko J (2009) A pre-hardened plastic mould steel with higher hardness. The 8th International Tooling Conference, Aachen, Germany, June 2-4, 2009

4. Mesquita RA, Barbosa CA (2005) 40 HRC plastic mould steels: Manufactuting properties considerations. Proceedings of 18th International Congress of Mechanical Engineering, Ourto Preto, MG, 6-11 November 2005.
5. Chandrasekaran H (1998) Machinability of ferrous alloys and the role of microstructural parameters-A litterature survey. Report IM-3664, Swedish Institute for Metals Research, Stockholm
6. Chandrasekaran H, M'Saoubi R, Karlsson O, Persson U (2005) Milling of prehardened mould steels- Role of microstructure on machinability and tool wear mechanisms. Report IM-2005-520, Swedish Institute for Metal Research, Stockholm
7. Akasawa T, Fukuda I, Nakamura K, Tanaka T (2004) Effect of microstructure and hardness on the machinability of medium-carbon chrome-molybdenum steel. J Mater Process Technol 143-144:66-71
8. M'Saoubi R, Chandrasekaran H (2004) Role of phase and grain size on chip formation and material work hardening during machining of single and dual phase steels. Ironmak Steelmak 31 (3):258-264
9. Jiang L, Roos Å, Liu P (1997) The Influnece of Austenite Grain Size and its Distribution on Chip Deformation and Tool Life during Machining of AISI 304L. Metall Mater Trans A 28A:2415-2422
10. Mian AJ, Driver N, Mativenga PT (2009) Micromachining of coarse-grained multi-phase material. Proceedings of the Institution of Mechanical Engineers Part B, J Eng Manuf 223:377-385. doi:10.1243/09544054JEM1185
11. Simoneau A, Ng E, Elbestawi MA (2006) Chip formation during microscale cutting of a medium carbon steel. Int J Mach Tool Manuf 46:467-481
12. Insausti A, M'Saoubi R (2002) Role of phase on material deformation of steels. Part II. Results from chip parameters, cutting forces and surface integrity studies. Report IM 2002013, Swedish Institute for Metal Research, Stockholm
13. Thoors H (1987) Effect of austenite grain size on machinability of a micro-alloyed forging steel (in Swedish). Report IM-2309, Swedish Institute for Metal Research, Stockholm
14. Vojcak ED (1992) The interaction of metallurgical conditions of low carbon steel on tool wear of a high speed steel. Proceedings of the Materials Issues in Machining and the Physics of Machining Processes, pp. 27-38
15. Hoseiny H, Klement U, Sotskovszki P, Andersson J (2011) Comparison of the microstructures in continuous-cooled and quench-tempered pre-hardened mould steels. Mater Des 32 (1):21-28
16. Luo Y, Wu X-c, Wang H-b, Min Y-a (2009) A comparative study on non-quenched and quenched prehardened steel for large section plastic mould. J Mater Process Technol 209:5437–5442. doi:10.1016/j.jmatprotec.2009.04.019
17. Marder AR, Krauss G (1967) The morphology of martensite in iron-carbon alloys. Trans ASM 60:651-660
18. Marder JM, Marder AR (1969) The morphology of iron-nickel massive martensite. Trans ASM 62:1-10
19. Morito S, Huang X, Furuhara T, Maki T, Hansen N (2006) The morphology and crystallography of lath martensite in alloy steels. Acta Mater 54:5323-5331
20. Morito S, Saito H, Ogawa T, Furuhara T, Maki T (2005) Effect of austenite grain size on the morphology and crystallography of lath martensite in low carbon steels. ISIJ Int 45 (1):91-94
21. Morito S, Tanaka H, Konishi R, Furuhara T, Maki T (2003) The morphology and crystallography of lath martensite in Fe-C alloys. Acta Mater 51:1789-1799

22. Furuhara T, Takayama N, Miyamoto G (2010) Key factors in grain refinement of martensite and bainite. Mater Sci Forum 638-642:3044-3049
23. Kitahara H, Ueji R, Tsuji N, Minamino Y (2006) Crystallographic features of lath martensite in low carbon steel. Acta Mater 54:1279-1288
24. Maki T, Tsuzaki K, Tamura I (1980) The morphology of microstructure composed of lath martensites in steels. Trans ISIJ 20:207-214
25. Morito S, Yoshida H, Maki T, Huang X (2006) Effect of block size on the strength of lath martensite in low carbon steels. Mater Sci Eng, A 438-440:237-240
26. Wang C, Wang M, Shi J, Hui W, Dong H (2008) Effect of microstructural refinement on the toughness of low carbon martensitic steel. Scripta Mater 58 (6):492-495
27. Krauss G (2001) Deformation and fracture in martensitic carbon steels tempered at low temperatures. Metall Mater Trans A 32A:861-877
28. García de Andrés C, Bartolomé MJ, Capdevila C, San Martín D, Caballero FG, López V (2001) Metallographic techniques for the determination of the austenite grain size in medium-carbon microalloyed steels. Mater Charact 46 (5):389-398
29. García de Andrés C, Caballero FG, Capdevila C, San Martín D (2003) Revealing austenite grain boundaries by thermal etching: advantages and disadvantages. Mater Charact 49:121-127
30. San Martín D, Palizdar Y, Cochrane RC, Brydson R, Scott AJ (2010) Application of Nomarski differential interference contrast microscopy to highlight the prior austenite grain boundaries revealed by thermal etching. Mater Charact 61 (5):584-588
31. Hjelen J, Tolleshaug BI (1992) Electron channeling contrast (ECC) imaging using specimen current. Micron and Microsc Acta 23 (1-2):179-180
32. Lloyd GE (1987) Atomic number and crystallographic contrast images with the SEM: a review of backscattered electron techniques. Mineral Mag 51:3-19
33. Medvedeva A, Bergström J, Gunnarsson S, Krakhmalev P, Nordh LG (2011) Influence of nickel content on machinability of a hot-work tool steel in prehardened condition. Mater Des 32 (2):706-715
34. Chandrasekaran H, M'Saoubi R, Högman B, Nordh L-G, Coulon B, Lebrun JL, Viale D, Gitton S, Montero MC, Marques MJ, Outeiro J, Dias A (2005) Development of machinability enhanced tool steels for improved product economy in hard milling. Technical Steel Research, Report EUR 21726. European Commission, Luxembourg
35. Sinha AK (2003) Physical Metallurgy Handbook. McGraw-Hill, New York
36. Smallman RE, Bishop RJ (1999) Modern Physical Metallurgy and Materials Engineering - Science, Process, Applications (6th Edition). Butterworth Heinemann, Oxford
37. Tomita Y, Okabayashi K (1986) Effect of microstructure on strength and toughness of heat-treated low alloy structural steels. Metall Mater Trans A 17A:1203-1209
38. Liu CD, Kao PW (1992) Tensile properties of a 0.34C-3Ni-Cr-Mo-V steel with mixed microstructure of lower-bainite-martensite structures. Mater Sci Eng, A 150:171-177

39. Ibaraki S, Takuya S (2010) A long-term control scheme of cutting forces to regulate tool life in end milling processes. Precis Eng 34:675-682
40. Trent EM, Wright PK (2000) Metal Cutting. 4 edn. Butterworth-Heinemann, Boston
41. Childs T, Maekawa K, Obikawa T, Yamane Y (2000) Metal Machining, Theory and Applications. Arnold, London
42. Bäker M (2006) Finite element simulation of high-speed cutting forces. J Mater Process Technol 176 (1-3):117-126
43. Tomota Y, Narui A, Tsuchida N (2008) Tensile behavior of fine-grained steels. ISIJ Int 48 (8):1107-1113
44. Ding T, Zhang S, Wang Y, Zhu X (2010) Empirical models and optimal cutting parameters for cutting forces and surface roughness in hard milling of AISI H13 steel. Int J Adv Manuf Technol 51:45-55
45. Olovsjö S, Wretland A, Sjöberg G (2010) The effect of grain size and hardness of wrought Alloy 718 on the wear of cemented carbide tools. Wear 268:1045-1052

Tables:

Table 1 Chemical composition of studied steel (wt%)

C	Si	Mn	P	S	Cr	Ni	Mo	V	Fe
0.39	0.27	1.36	0.017	0.006	1.95	1.0	0.27	0.06	bal.

Table 2 Cutting conditions used for the machining experiments

Cutting speed, V_c (m/min)	120 - 200
Feed per tooth, f_z (mm/rev)	0.2
Number of inserts, N_t	1
Axial depth of cut, d_c (mm)	1
Radial depth of cut, a_e (mm)	14
Coolant	Dry

Table 3 Mechanical properties of investigated heat treated steel specimens at room temperature. $R_{p0.2}$: Yield Strength; R_m: Tensile Strength; A_5: Elongation; Z: Area Reduction; CVN: Charpy-V Impact Toughness; The error is the standard deviation of mean value

T_γ (°C)	$R_{p\,0.2}$ (MPa)	R_m (MPa)	$R_m/R_{p\,0.2}$	A_5 (%)	Z (%)	CVN (J)
900	1219 ± 15	1347 ± 16	1.10 ± 0.003	12 ± 1	47 ± 16	13.7 ± 1
950	1226 ± 3	1375 ± 2	1.12 ± 0.002	11 ± 1	44 ± 4	12.5 ± 1.3
1000	1209 ± 2	1363 ± 2	1.13 ± 0.000	10 ± 0	39 ± 2	10.9 ± 1.2
1050	1208 ± 4	1373 ± 3	1.14 ± 0.002	9 ± 0	31 ± 1	8.3 ± 1.1

Figure captions:

Fig. 1 Optical micrographs of thermally etched samples after heating to different austenitization temperatures (a) 900 ºC, (b) 950 ºC, (c) 1000 ºC and (d) 1050 ºC. The location of some prior austenite grain (thick arrows) and twin (thin arrows) boundaries has been highlighted

Fig. 2 Electron Channeling Contrast (ECC) images of the specimens austenitized at (a) 900˚C; (b) 950˚C; (c) 1000˚C and (d) 1050˚C after quenching and tempering. Examples of the location of prior austenite grain (white solid lines) and packet (white dotted lines) boundaries have been highlighted

Fig. 3 (a) The size of prior austenite grains and martensitic packets obtained by austenitizing at different temperatures (T_γ). The error bar is standard deviation. (b) The correlation between the average prior austenite grain and packet size

Fig. 4 FEG-SEM micrographs of quenched and tempered samples after austenitization at (a) 900˚C (b) 950˚C, (C) 1000˚C and (d) 1050˚C showing the M_3C precipitates inside the martensitic lath (thin arrows) and on the lath boundaries (thick arrows)

Fig. 5 Variation of the resultant cutting force (F_{xy}) with (a) packet size and (b) cutting speed (V_c)

Fig. 6 Work hardening ratio ($R_m/R_{p0.2}$) vs. reciprocal square root of packet size (d_p)

Fig. 7 Maximum flank wear evolution on cutting tool edge vs. milling time at cutting speeds (V_c) of (a) 120 m/min, (b) 160 m/min, (c) 200 m/min and different heat treatments; (d) variation of cutting force amplitude with austenitization temperature (T_γ) at the cutting speed of 120 m/min

Fig. 8 Microscopic view of flank wear and notch wear on the insert used for milling the material austenitized at 900˚C at the cutting speed of 120 m/min

Figure 1

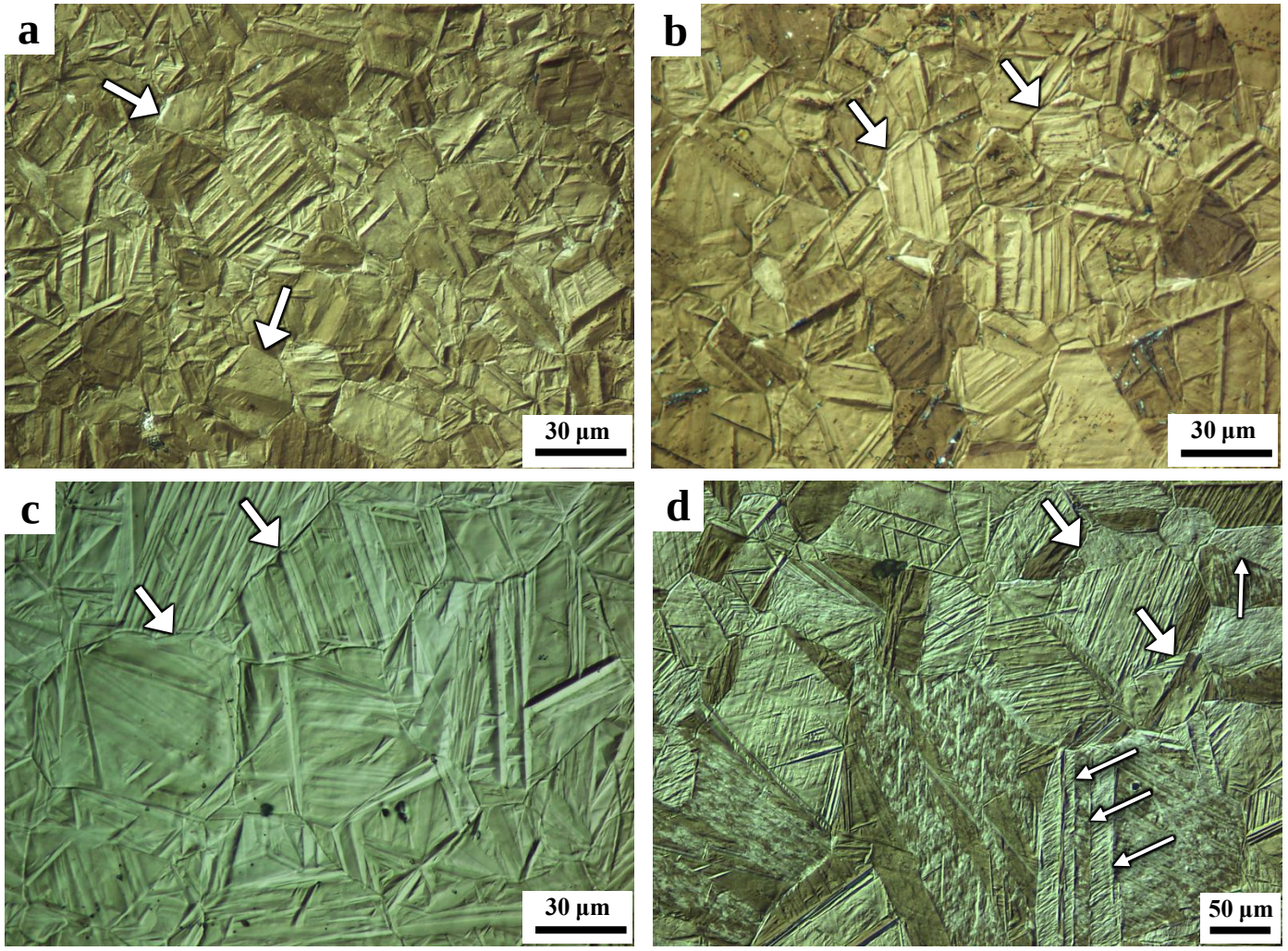

Figure 2

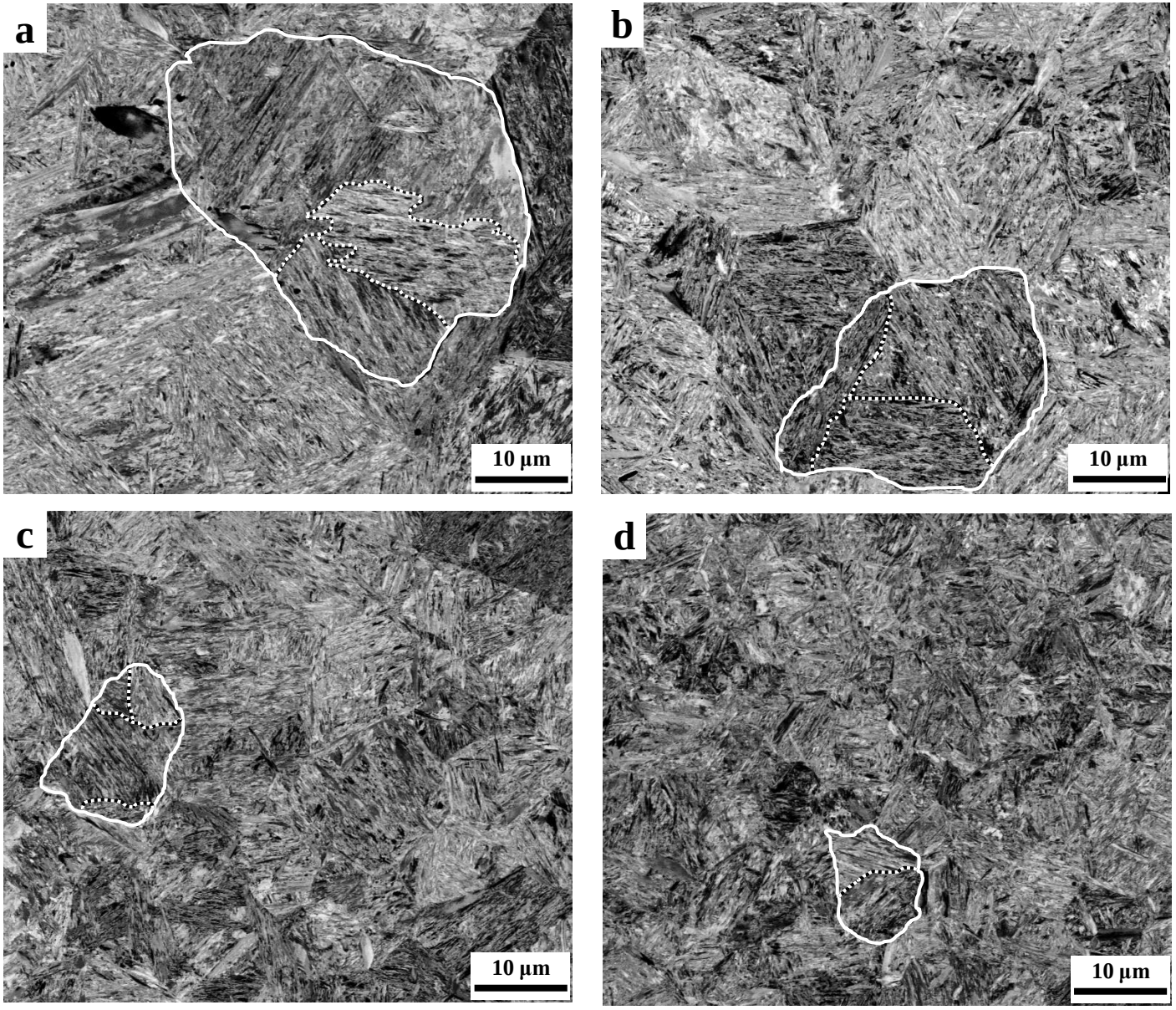

Figure 3

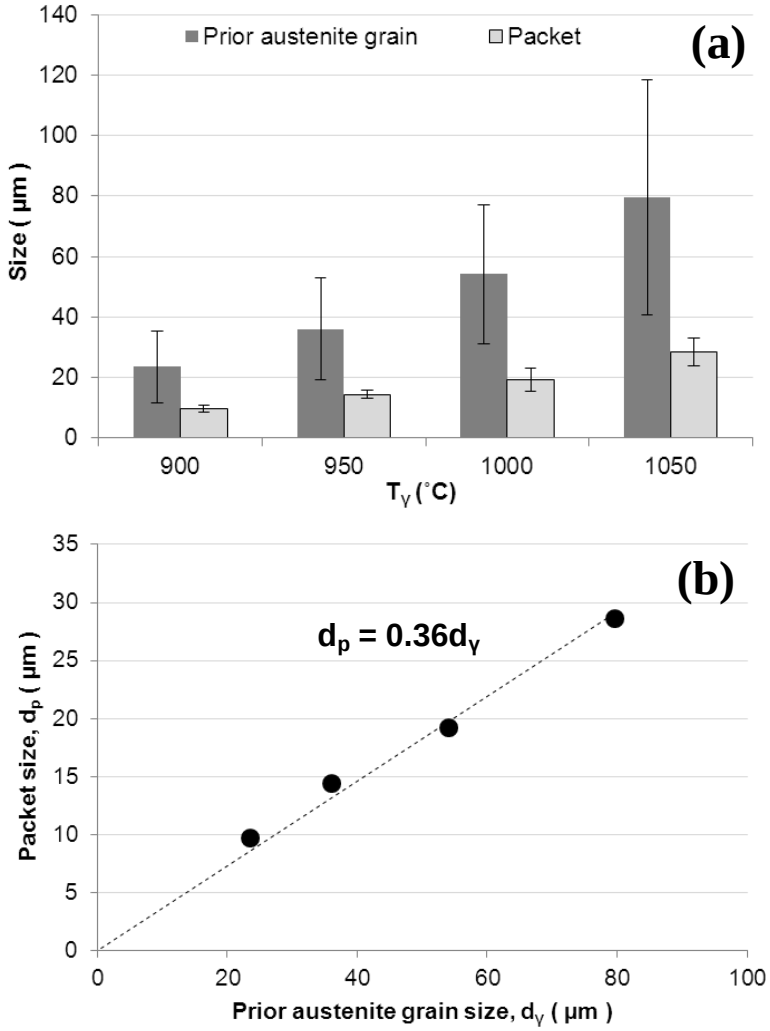
(a)
Prior austenite grain
Packet
Size (μm)
140
120
100
80
60
40
20
0
900
950
1000
1050
T_γ (°C)
(b)
$d_p = 0.36d_\gamma$
Packet size, d_p (μm)
35
30
25
20
15
10
5
0
0
20
40
60
80
100
Prior austenite grain size, d_γ (μm)

Figure 4

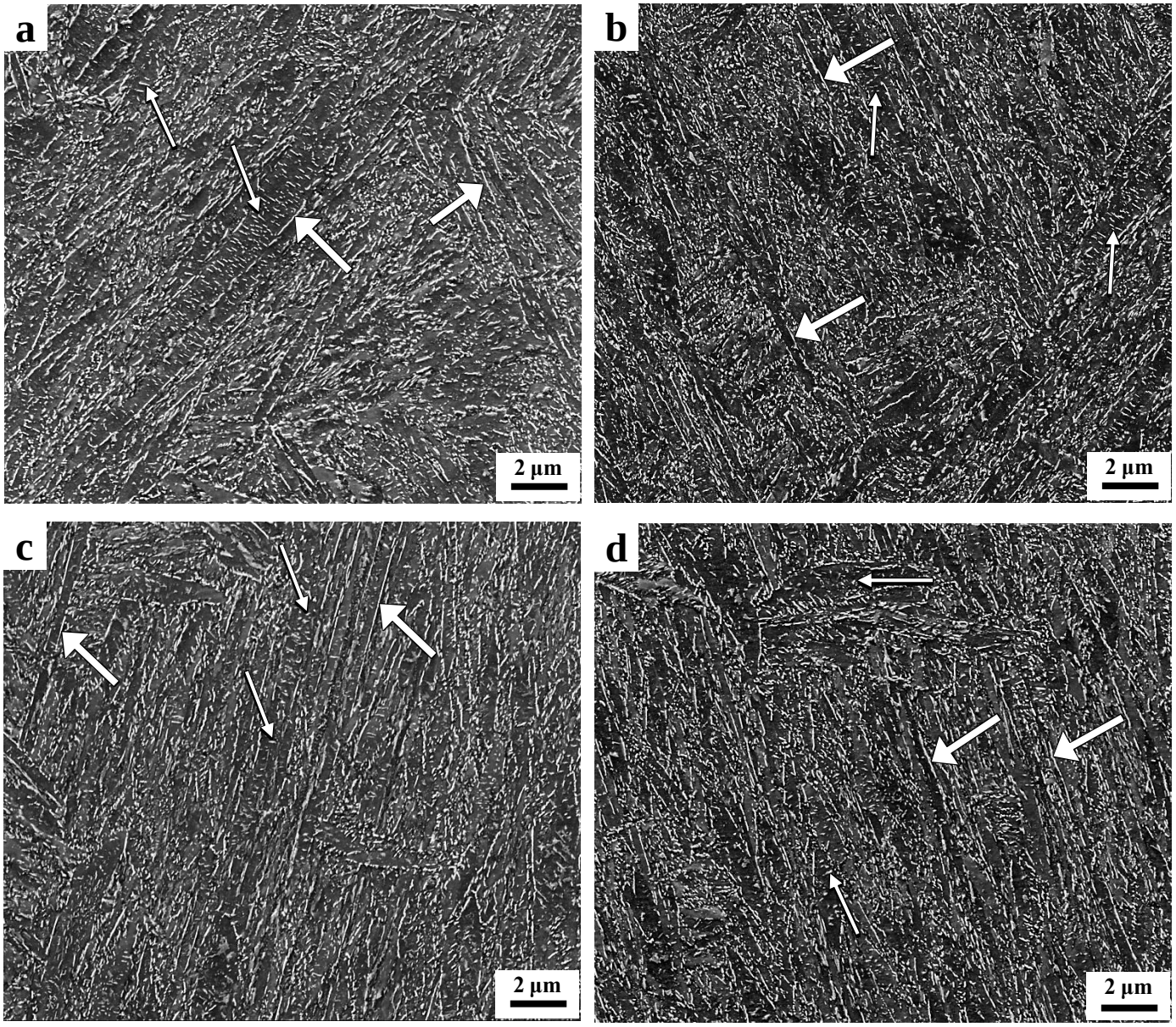

Figure 5

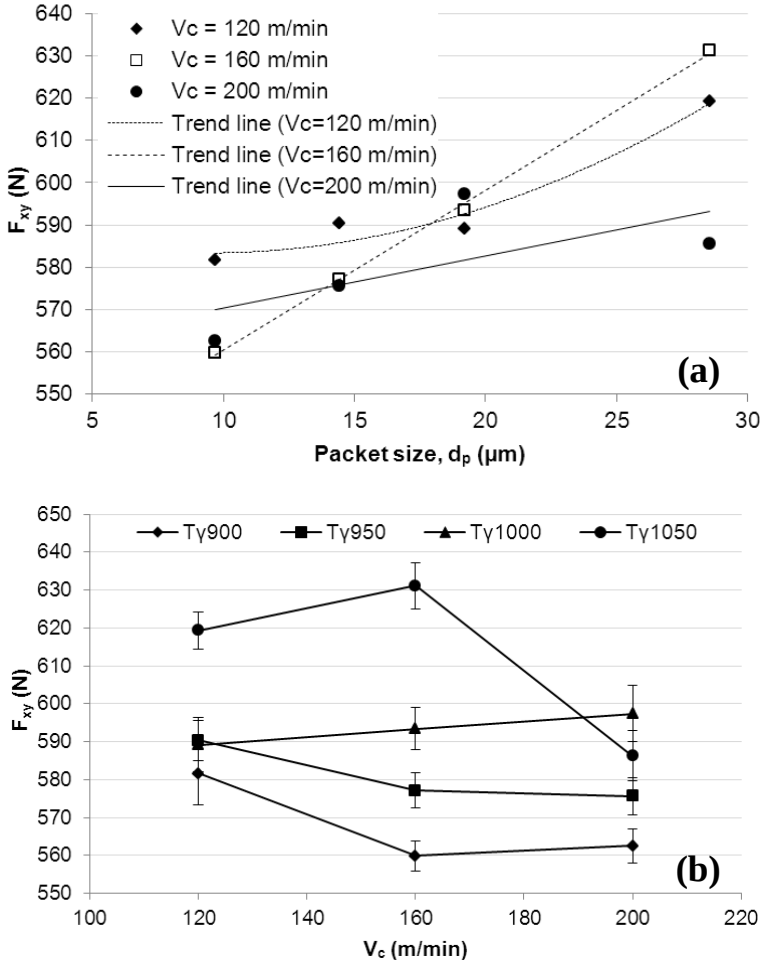
Vc = 120 m/min
Vc = 160 m/min
Vc = 200 m/min
Trend line (Vc=120 m/min)
Trend line (Vc=160 m/min)
Trend line (Vc=200 m/min)
F_{xy} (N)
Packet size, d_p (μm)
(a)
Tγ900
Tγ950
Tγ1000
Tγ1050
F_{xy} (N)
V_c (m/min)
(b)

Figure 6

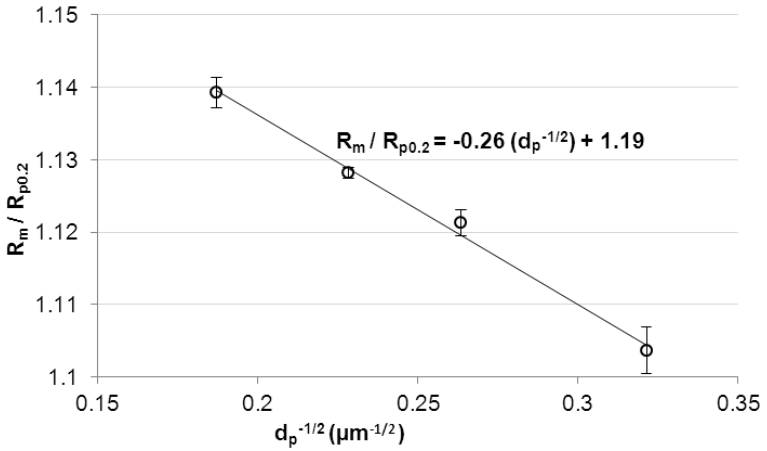
1.15
1.14
1.13
1.12
1.11
1.1
0.15
0.2
0.25
0.3
0.35
$R_m / R_{p0.2} = -0.26 (d_p^{-1/2}) + 1.19$
$R_m / R_{p0.2}$
$d_p^{-1/2}$ ($\mu m^{-1/2}$)

Figure 7

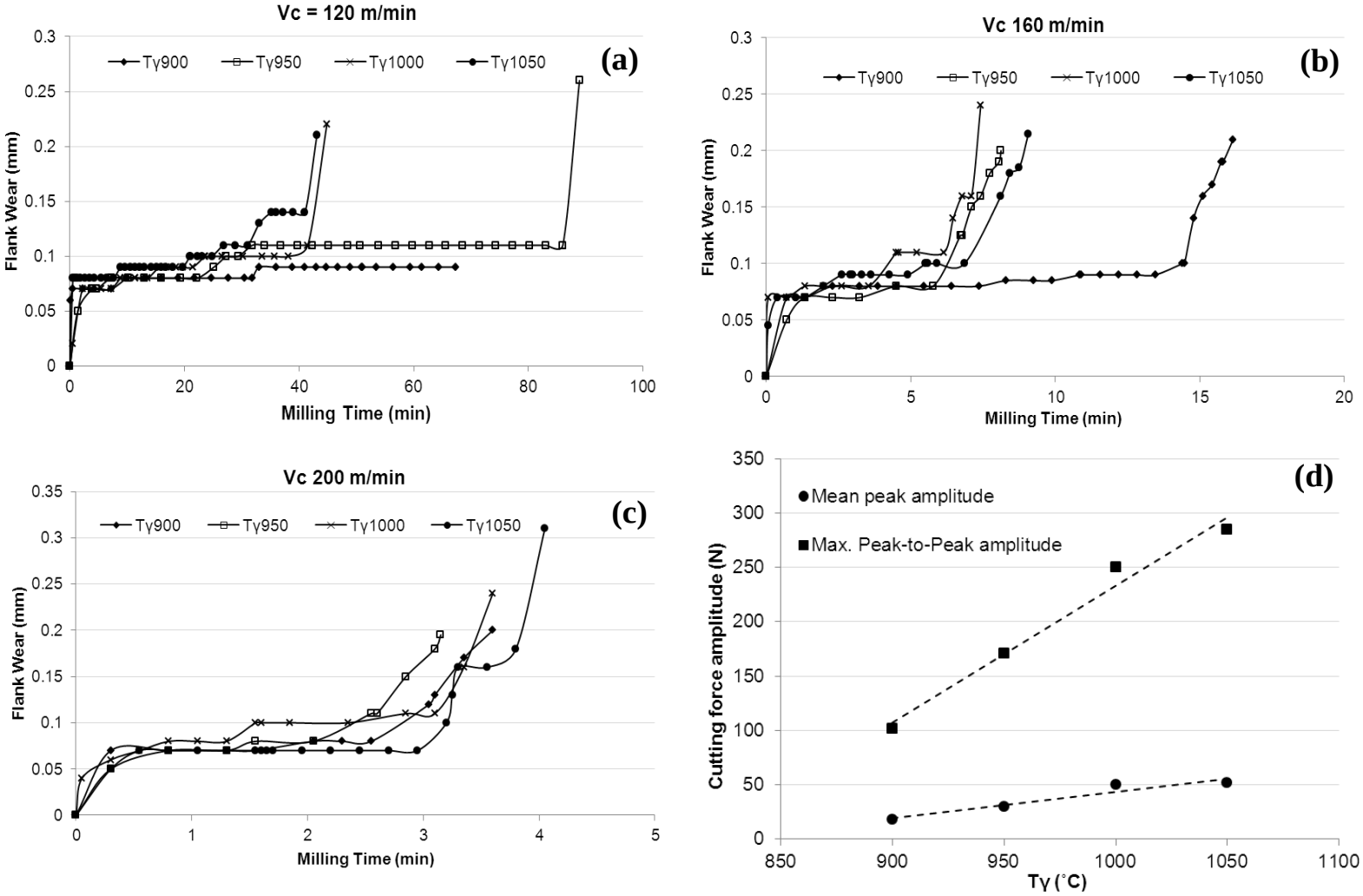
Vc = 120 m/min
(a)
Tγ900
Tγ950
Tγ1000
Tγ1050
Flank Wear (mm)
Milling Time (min)
Vc 160 m/min
(b)
Tγ900
Tγ950
Tγ1000
Tγ1050
Flank Wear (mm)
Milling Time (min)
Vc 200 m/min
(c)
Tγ900
Tγ950
Tγ1000
Tγ1050
Flank Wear (mm)
Milling Time (min)
(d)
Mean peak amplitude
Max. Peak-to-Peak amplitude
Cutting force amplitude (N)
Tγ (˚C)

Figure 8